California Polytechnic State University
San Luis Obispo, CA 93407

14P

Numerical Investigation of Multi-Element Airfoils

Final Technical Report
October 1993

NASA Cooperative Agreement NCC 2-761

Russell M. Cummings
Aeronautical Engineering Department

The final technical report for this project is enclosed as an AIAA technical meeting paper entitled, "Navier-Stokes Analysis of Lift-Enhancing Tabs on Multi-Element Airfoils," AIAA Paper 94-0050, which will be presented at the AIAA 32nd Aerospace Sciences Meeting in Reno, January 1994. The paper has also been submitted for consideration to the *Journal of Aircraft*.

AIAA 94-0050

Navier-Stokes Analysis of Lift-Enhancing Tabs on Multi-Element Airfoils

Paul G. Carrannanto
Ford Motor Company

Bruce L. Storms
Sterling Software

James C. Ross
NASA Ames Research Center

Russell M. Cummings
California Polytechnic State University

32nd Aerospace Sciences Meeting & Exhibit
January 10-13, 1994 / Reno, NV

NAVIER-STOKES ANALYSIS OF LIFT-ENHANCING TABS ON MULTI-ELEMENT AIRFOILS

Paul G. Carrannanto*
Advanced Vehicle Systems Engineering, Ford Motor Company

Bruce L. Storms†
Sterling Software
Moffett Field, CA 94035

James C. Ross††
Fixed Wing Aerodynamics Branch, NASA Ames Research Center
Moffett Field, CA 93405

Russell M. Cummings**
Aeronautical Engineering Department, California Polytechnic State University
San Luis Obispo, CA 93407

Abstract

The flow over multi-element airfoils with flat-plate lift-enhancing tabs was numerically investigated. Tabs ranging in height from 0.25% to 1.25% of the of the reference airfoil chord were studied near the trailing edge of the main-element. This two-dimensional numerical simulation employed an incompressible Navier-Stokes solver on a structured, embedded grid topology. New grid refinements were used to improve the accuracy of the solution near the overlapping grid boundaries. The effects of various tabs were studied at a constant Reynolds number on a two-element airfoil with a slotted flap. Both computed and measured results indicated that a tab in the main-element cove improved the maximum lift and lift-to-drag ratio relative to the baseline airfoil without a tab. Computed streamlines revealed that the additional turning caused by the tab may reduce the amount of separated flow on the flap. A three-element airfoil was also studied over a range of Reynolds numbers. For the optimized flap rigging, the computed and measured Reynolds number effects were similar. When the flap was moved from the optimum position, numerical results indicated that a tab may help to reoptimize the airfoil to within 1% of the optimum flap case.

Nomenclature

Symbols

α	angle-of-attack, deg.
c	reference airfoil chord
C_d	section drag coefficient $\equiv D / q_\infty c$
C_l	section lift coefficient $\equiv L / q_\infty c$
C_p	pressure coefficient $\equiv (p - p_\infty) / q_\infty$
D	drag
δ	deflection angle
h	tab height
d	distance from tab to trailing-edge
L	lift
L / D	lift-to-drag ratio
M	Mach number
q	dynamic pressure $= \frac{1}{2}\rho V^2$
ρ	air density
R_e	Reynolds number

Subscripts

f	flap
∞	freestream condition
max	maximum
s	slat

Introduction

High-lift aerodynamics continues to play an important role in the design of new aircraft. Improved high-lift performance can lead to increased range and payload or decreased landing speed and field length requirements. Hence, there is a continuous need to improve the maximum lift and lift-to-drag ratio (L / D) of the high-lift system. Much of the optimization work is performed in two-dimensional (2D) wind-tunnel studies of multi-element airfoils. Even in two-dimensions, however, the effects of Reynolds and Mach numbers can be significant, making it difficult to predict the full-scale aircraft performance at maximum lift conditions.[1-3] Reliable computational methods could help reduce the amount of expensive wind-tunnel testing required, while providing some insight into the complex flow physics. In this paper, novel Gurney-type flap devices were numerically investigated on multi-element airfoil systems.

---

* Product Design Engineer. Formerly Graduate Research Assistant, Aeronautical Engineering Department, California Polytechnic State University, San Luis Obispo, CA 93407. Member AIAA.

† Aerospace Engineer. Member AIAA.

†† Aerospace Engineer. Senior Member AIAA.

** Department Chair and Professor. Associate Fellow AIAA.

The Gurney flap is a flat plate device which is mounted perpendicular to the trailing edge of the furthest downstream wing element (Fig. 1). The Gurney flap was originally used on race car wings to increase the down-force needed for lateral traction. As Liebeck first hypothesized,[4] a Gurney flap increased the lift by deflecting the flow at the trailing edge of an airfoil.

A Gurney-type flap device suitable for aircraft applications must be stowable during cruise operation. This can be achieved by mounting the device on a hinge mechanism slightly inboard from the trailing edge (Fig. 2). This lift-enhancing tab[5] resembles a Gurney flap, but its placement is not limited to last wing element. In fact, the tab can be mounted on any airfoil element which could benefit from additional aft camber. When mounted between adjacent airfoil elements (Fig. 2), the tab also modifies the effective gap. This could potentially alleviate adverse Reynolds number effects due to the slot flow.[3] This is desirable, because such Reynolds number effects can reduce the performance of an aircraft high-lift system relative to that measured in wind-tunnel testing.

Lift-enhancing tabs were tested[5] near the trailing edge of the main-element on a two-element airfoil, as shown in Fig. 2. Wind-tunnel measurements showed that the tab increased the loading on the main-element and delayed the flow separation on the flap, which significantly increased the maximum lift and L/D generated by the airfoil. A variety of tab arrangements were tested, and the highest performance was achieved with a tab height of 0.5%-chord, rather than 1%-chord. This result is somewhat different than the results obtained by other researchers[6-8] for Gurney flaps. In those studies, maximum lift generally increased with Gurney flap height, while L/D decreased for heights larger than about 2%-chord. With lift-enhancing tabs, however, maximum lift and L/D were both nearly optimum for the same tab height.

In order to design such a tab for a multi-element airfoil system, it is desirable to compute its effects at maximum lift conditions. Due to the strongly viscous behavior of multi-element airfoils and Gurney-type flap devices, a Navier-Stokes code is required. Rogers[9,10] has simulated multi-element airfoils (without tabs) using INS2D-UP[11] and the Chimera[12] embedded grid scheme. The computations were highly accurate in predicting the maximum lift of a three-element airfoil. Predictions for Reynolds number effects showed good qualitative results, but the drag was somewhat less predictable. That method is extended here by placing lift-enhancing tabs near the trailing edges of the airfoil elements.

In deployed position, the tab resembles a Gurney flap. Hence, the method of simulating the tab is very similar to a previous study, by Jang et al.,[13] of Gurney flaps on a single-element NACA 4412 airfoil. Those INS2D-UP computations predicted accurate trends for the increase in lift and nose-down pitching-moment due to the various-sized Gurney flaps. Again, the predicted drag increment was somewhat less accurate.

The goal of the current study was to predict the change in aerodynamic coefficients due to the tabs. A grid refinement was performed to improve the accuracy of the solution near the overlapping grid boundaries. Computations for a two-element airfoil with and without a tab were validated with wind tunnel data.[5] Several more tab heights were numerically investigated in order to optimize the maximum lift coefficient. A three-element airfoil was also studied over a range of Reynolds numbers. The computed results were compared with experimental data for the airfoil without a tab.

Numerical Investigation

Flow Solver

The incompressible Navier-Stokes code, INS2D-UP,[11] was selected for this analysis. Compressibility effects were neglected, due to the low freestream Mach numbers ($M_\infty \approx 0.2$) for an aircraft in landing configuration. INS2D-UP employs the method of artificial compressibility to couple the pressure and velocity fields. The convective fluxes are upwind-differenced using a third-order flux-difference splitting technique, while the viscous fluxes are central-differenced in standard second-order form. The resulting equations are solved with an implicit line-relaxation scheme, which provides high convergence rates for steady-state problems and for the sub-iterations in time-dependent problems. In this study, fully-turbulent computations were performed using the one-equation Baldwin-Barth turbulence model.[14]

Geometry and Boundary Conditions

The two-element airfoil geometry is shown in Fig. 3, and the boundary conditions for the INS2D-UP simulation are shown in Fig. 4. For simplicity, the computations assumed freestream farfield conditions, and the experimental data was corrected for the effects of the wind tunnel walls. A grid sensitivity study verified that the effect of the freestream assumption was negligible for farfield radii greater than about 10-chords. Hence, the farfield and outflow boundaries were placed at least 10-chords away from the airfoil surface as shown. At the outflow boundary, the velocity was extrapolated, assuming a uniform static pressure distribution. No-slip wall boundary conditions are applied at the airfoil surface. The coincident points along the wake-cut are updated by averaging values from the surrounding points.

Grid Generation and Refinement

A close-up of the two-element airfoil grid is shown in Fig. 5. The grids used in this study were modeled after Rogers[9,10] structured Chimera grids for multi-element airfoils. This procedure utilizes an overlapping grid system to combine the different grids into a composite mesh. C-Grids were generated individually for the main-element and flap using the HYPGEN code.[15] Grid points were clustered in the boundary layer, with normal grid spacings of 1×10^{-5} chords ($y^+ \approx 1$) at the surface. The number of grid points were 307 streamwise by 98 normal for the main-element and 155 x 42 for the flap .

The two grids were overlaid using the PEGSUS code.[16] In this technique, each C-grid is treated as a different zone, and holes are cut in each grid to accommodate the adjacent zonal boundaries. As shown in Fig. 5, the flap grid zone is embedded inside the main-element, and the main-element extends to the farfield boundary. In the composite mesh, the grids are allowed to overlap, and numerical interpolation is used to transmit information across these zonal boundaries.

The surface of the baseline airfoil (without tabs) forms the inner boundary of the computational domain. In order to model the tabs, INS2D-UP has the capability to create no-slip wall boundaries on the interior of the mesh. This boundary condition was used to "blank-out" grid points at the desired tab locations as shown in Fig. 6. This feature enabled a variety of tab heights and locations to be studied using the same grid.

Due to the small dimensions of a tab ($h \approx 1\%$-chord), grid points were clustered in this region. The normal and streamwise spacings were 0.0005 and 0.001 chords, respectively, as shown in Fig. 6. Computed streamlines revealed that this grid resolution was fine enough to resolve the dominant recirculating flow structures near the tab. Although it would be desirable to have boundary layer resolution along the tab surfaces, this would significantly increase the overall grid dimensions and also complicate the grid generation for a study of different tab heights and locations.

The initial flow solutions revealed that additional grid refinement was necessary to resolve regions of high-shear flow near a Chimera zonal boundary. An example of this problem can be in Fig. 7, which shows the overlap regions around the flap for an initial grid. A hole is cut in the main-element grid (solid lines) to accommodate the flap grid (dotted lines). This hole-cut creates fringe points (larger dots) in the main-element grid, which receive information by interpolation from the flap grid. In this region, however, the high-shear wake flow from the flap must pass into the main-element grid. Notice that the main-element grid cells are locally much coarser than the flap cells. Neither fringe point is in line with the flap wake. Hence, the velocity deficit in the flap wake does not properly pass into the main-element grid when the interpolation is performed. This creates errors in the velocity magnitude and direction at the fringe points. Rogers[10] noted a similar problem in the vicinity of the slat trailing edge for a three-element airfoil. The problem may lead to erroneously high pressure coefficients upstream of the trailing edge.

More fringe points are needed in this high-shear flow region. Hence, many refinement techniques were applied to the final grid (Fig. 8). Elliptic smoothing[10] was applied to the flap grid to increase the normal spacing of the grid lines aft of the trailing edge. This smoothing spread the flap grid lines outward from the trailing edge and also redistributed the cells more evenly across the hole-cut. The reduced aspect ratio of these cells also enhanced the convergence in the flap wake region. In addition, the normal grid density in the main-element was also significantly increased in the wake-cut region. This clustered many more fringe points across the hole-cut and improved the interpolation of information from the flap grid.

Several new techniques were also used to improve the interpolation. One method was to move the hole-cut boundary further downstream from the flap trailing edge. This allowed the flap wake to dissipate and thicken before reaching the hole-cut boundary. The velocity deficit was then passed smoothly into the main-element grid. Similar refinement was applied to all of the high-shear flow regions near the Chimera hole-cut boundaries, such as near the lift-enhancing tabs. Another technique was to prescribe the main-element wake cut line to be parallel to the flap (Fig. 9). This insured that the flap grid cells overlapped into the highest density region in the main-element grid. This procedure was useful for studying a variety of flap angles. A new main-element grid was quickly generated for each flap angle, since only the shape of the wake-cut required modification.

Results and Discussion

Two-Element Airfoil

The two-element airfoil geometry (Fig. 3) consists of a NACA 63_2-215 Mod B airfoil[17] with a 30%-chord single-slotted flap. This airfoil was tested at the 7x10-Foot Wind Tunnel #2 at NASA Ames Research Center.[5] The flap was deflected at 43.5°, with a 3.1%c gap and 4.2%c overlap, defined as shown. The 2D model was mounted between false walls across the 7 foot dimension of the test section. Boundary layer control was used to minimize the 3D effects of the false walls. Wind tunnel wall corrections were applied to the experimental data. This data was used to validate the current CFD results for the effects of lift-enhancing tabs. The two-element airfoil (without a tab) was used as the baseline geometry for the INS2D-UP simulation. All computations were performed at a Reynolds number of 3.7 million to match the experiment.

Figure 10 shows a comparison of the measured and computed pressure distributions for the airfoil at approximately 8.5° angle-of-attack. For the baseline airfoil in Fig. 10a, the computed pressures agreed well with the measured data, except for slightly under predicting the suction on the upper surface of the main-element. The calculations also did an excellent job of predicting the separation point on the flap. The flow separation is indicated by the flattening of the pressure curve on the upper surface of the flap, which occurs at approximately 10% of the flap chord. The discrepancy between the measured and computed lift coefficient for this case was less than 3.9%.

A similar plot is shown in Fig. 10b for the airfoil with a 1%c tab located at 1%c from the main-element trailing edge. Excellent agreement between the computed and measured pressure is seen on the main-element and flap. The discrepancy in lift coefficient for this case was less than 1.5%. The 1%c tab significantly increased the loading on the main-element relative to the baseline airfoil, particularly near the trailing edge. The tab also suppressed the large suction peak near the leading edge of the flap, which was seen on the baseline case. The lower suction peak weakened the adverse pressure gradient and allowed the boundary layer to remain attached along the entire length of the flap. The overall effect of the tab was an increase in lift coefficient relative to the baseline airfoil. The computed increase of 17% was close to the measured 15% increase.

Particle traces were used to visualize the computed streamlines over the airfoil with and without the 1%c tab. Figure 11a shows a close-up of the slotted flap on the baseline airfoil. The flow exited the slot parallel to the main-element trailing edge and minimal turning occurred as the flow separated at about 10% of the flap chord. However, when the tab was placed in the cove (Fig. 11b), the streamlines were turned downward by approximately 20° at the main-element trailing edge. This turning reduced the effective angle of attack of the flap, which weakened the adverse pressure gradient and caused the boundary layer to reattach along the entire length of the flap. This effect was similar to adding camber to the trailing edge of the main-element. Immediately downstream of the tab, there was a contrarotating recirculation region which resembled Liebeck's[4] hypothesized flowfield diagram for a Gurney flap (Fig. 1). Further downstream, the wake from the main-element thickened and then reversed as it encountered the adverse pressure gradient above the flap. A similar off-surface separation was shown by Rogers computations for a three-element airfoil without tabs.[10] Even with the off-surface separation, the tab increased the overall lift of the airfoil.

The measured and computed lift and drag curves for the airfoil with and without the tab are compared in Fig. 12. In Fig. 12a, the lift curves are in good agreement at low angles of attack, where the lift curve is shifted by about 5° due to the tab. However, the slopes of the computed lift curves are slightly lower than measured. In addition, the computed maximum lift values and stall angles are higher than measured. This may be a result of the turbulence modeling and the lack of a transition model in the fully-turbulent computations.[10] However, the computations do reflect the correct direction in changes due to the tab. The computations show a 5.2% increase in maximum lift due to the tab, which is close to the measured value of 3.9%. The computations also matched the measured results for the 3° reduction in angle of attack at maximum lift due to the tab.

The measured and computed drag polars are compared in Fig. 12b. The agreement is good at low lift coefficients for the airfoil with and without the tab. As lift coefficient increases, the computations predict higher drag values than were measured. The measured maximum lift-to-drag ratio was increased by 13% compared to a computed increase of only 4.6%. However, the computations were accurate in showing that the tab reduced the drag at the moderate lift coefficients. Although the exact values of lift and drag were not matched, the computations do show the correct sign in the directional changes due to the tab. This makes the computations useful as a design tool.

Several more tab heights and locations were numerically investigated on the main-element. A constant angle of attack of 13° was selected for this study, because this was approximately the maximum lift angle for the tab heights previously studied. The computations indicated that the tabs performed best when placed at the trailing edge rather than slightly inboard. Hence, all subsequent computations were performed with the tabs at the trailing edge. The computed and measured lift variation with tab height is shown in Fig. 13. The computations show that the optimum tab height is approximately 0.4%c for this airfoil and flap rigging. This result was consistent with the experimental data for the two tab heights, which showed that the maximum lift was highest with the 0.5%c tab. The ability to predict very close to the optimum tab height also makes the current computational method useful as a design tool.

Three-Element Airfoil

The three-element airfoil geometry is shown in Fig. 14. This Douglas transport airfoil consists of a slat and single-slotted flap. The 2D airfoil was tested at the Low-Turbulence Pressure Tunnel at NASA Langley Research Center.[1] Wind tunnel wall and boundary layer control corrections were applied to the data. The baseline airfoil (without tabs) was experimentally optimized for maximum lift at a Reynolds number of 9×10^6. The optimum settings for the slat were -30° deflection, with a 2.95%c gap and -2.5%c overlap, while the optimum flap settings were +30° deflection, with a 1.32%c gap and 1.0%c overlap. The optimized airfoil geometry from that test was used as the baseline geometry for the current computations.

The computational grid for the three-element airfoil is shown in Fig. 15. This grid was originally developed by Rogers for a study of several turbulence models.[10] For the present study, modifications were made to improve the grid resolution at the tab locations. The final grid had streamwise and normal dimensions of 121 x 31, 325 x 100, and 121 x 41, respectively, for the slat, main, and flap elements.

As a code validation case, the optimized configuration was computed at 4° angle of attack. Figure 16 shows good agreement between the computed pressure distribution and measured data from Ref. 1. Although the computed suction on the upper surface of the slat was slightly higher than measured, the discrepancy in total lift coefficient was less than 3.6%.

The maximum lift performance of multi-element airfoils may vary significantly with Reynolds number.[1-3] Figure 17 reflects this trend for the baseline airfoil, which was optimized at $R_c = 9$ million. The measured results show an approximate 2% reduction in maximum lift at the lower and higher Reynolds numbers.

The baseline airfoil was computed at 25° angle-of-attack over the same Reynolds number range. This angle of attack of was selected, since it was approximately the computed maximum lift angle. Although the absolute values of the computed lift coefficients were slightly higher than measured, the Reynolds number effects were similar, showing that the lift was highest at $R_c = 9$ million. All subsequent computations were also performed at 25° angle-of-attack.

The flap was moved from the optimum position in order to study the use of tabs for reoptimizing the performance. The flap gap was increased from 1.32%c to 2.18%c, and the deflection was increased from 30° to 45°. The effect of an oversized gap is similar to increasing the Reynolds number with a fixed gap. Maximum lift may decrease due to a reduction in favorable viscous interaction between the main-element and flap.[3] This is sometimes a problem when a multi-element airfoil is optimized at a low Reynolds number and then tested at full-scale; the gap may be too large and no longer optimum at the higher Reynolds number. However, a tab changes the effective gap of the slot.[5] Therefore, it may be possible to reoptimize the gap at a higher Reynolds number by using a tab.

The airfoil was numerically investigated in the non-optimum flap setting at 25° angle-of-attack. The computed lift at two Reynolds numbers is shown in Fig. 18. For the airfoil without a tab, the flow on the flap was separated at both Reynolds numbers. This significantly reduced the lift performance relative to the optimum flap case, as shown. There was a further reduction in lift ($\Delta C_l \approx -0.17$) at the higher Reynolds number, due to Reynolds number effects which may be associated with the separated flow.

In order to regain the lift performance for this non-optimum flap case, a tab was placed at the trailing edge of the main-element. Since the optimum gap had been increased by almost 0.9%c, tab heights ranging from 0.5%c to 1%c were initially considered. However, the numerical solutions at 25° angle-of-attack for tab heights larger than 0.5%c tended not to converge. This was probably due to computing slightly beyond the maximum lift angle-of-attack. The results for a 0.5%c tab are shown in Fig. 18. The lift coefficient oscillated within the bounds shown, and for illustration purposes, the average value was plotted. The 0.5%c tab significantly improved the averaged lift coefficient relative to the non-optimum case without a tab. At $R_c = 9$ million the averaged lift was also 4.9% higher than the optimum flap case without a tab. The large increase in lift was due to the flow reattaching on the upper surface of the flap, as in the case of the two-element airfoil. In addition, the 0.5%c tab virtually eliminated the Reynolds number effects which were seen for the airfoil without a tab. This suggested that the tab may help to reduce some of the Reynolds number sensitivity associated with the separated flow on the flap.

In order to verify the above results, smaller tab heights were considered. The converged solution for a 0.25%c tab at $R_c = 9$ million is shown in Fig. 18. The 0.25%c tab also improved the lift relative to the case without a tab. The lift coefficient was within 1% of the optimized flap case. This reaffirmed that a tab may help to reoptimize the airfoil with the flap in non-optimum position.

Conclusions

The effects of lift-enhancing tabs were numerically investigated on multi-element airfoil configurations. New grid refinement techniques were used to improve the accuracy of the solution near the overlapping grid boundaries. A two-element airfoil was investigated throughout a range of angles of attack. Although the computations did not match the absolute values for maximum lift, the magnitude and direction of changes due to the tab were consistent with the measured results. This makes the current method valuable as a design tool. Both computed and measured results indicated that a 1%c tab increased the loading on the main element and reattached the flow on the flap surface. Computed streamlines near the trailing edge revealed the additional turning caused by the tab. In addition, the optimal computed tab height of 0.4%c was consistent with the available experimental data.

For the optimized three-element airfoil, although the computations did not exactly match the measured values for maximum lift, the Reynolds number trends were similar. The flap was then moved away from the optimum position. This produced separated flow on the flap, causing a significant reduction in lift relative to the optimum flap case. The computations showed that a 0.25%c tab restored the lift to within 1% of the optimum flap case. Although numerical solutions for larger tab heights did not converge, higher lift potential was observed. These results suggest that a tab may help to reoptimize an airfoil with the flap in non-optimum position.

Acknowledgments

This research was supported by NASA Ames Research Center Grant No. NCC 2-761. The computer resources were supplied by the Fixed Wing Aerodynamics Branch and the Central Computing Facility at NASA Ames. The authors would like to thank Dr. Stuart E. Rogers of NASA Ames for his assistance throughout this investigation.

References

1. Valarezo, W. O., Dominik, C. J., McGhee, "Reynolds and Mach Number Effects on Multielement Airfoils," *Proceedings of the Fifth Numerical and Physical Aspects of Aerodynamic Flows*, Jan. 1992.

2. Mack, M. D. and McMasters, J. H., "High Reynolds Number Testing in Support of Transport Airplane Development," AIAA Paper 92-3982, 1992.

3. Woodward, D. S., Hardy, B. C., Ashill, P. R., "Some Types of Scale Effect in Low-Speed High-Lift Flows," 16th ICAS Congress, 1988.

4. Liebeck, R. H., "Design of Subsonic Airfoils for High Lift," *Journal of Aircraft*, Vol. 15, No. 9, Sept. 1978, pp. 547-561.

5. Ross, J. C., Storms, B. L., and Carrannanto, P. C., "Lift-Enhancing Tabs on Multi-Element Airfoils," AIAA Paper 93-3504, Aug. 1993.

6. Katz, J. and Largman, R., "Effect of 90 Degree Flap on the Aerodynamics of a Two-Element Airfoil," *Journal of Fluids Engineering*, Vol. 111, Mar. 1989, pp. 93-94.

7. Katz, J., and Dykstra, L., "Study of an Open-Wheel Racing Car's Rear Wing Aerodynamics," SAE Paper 890600, Feb. 1989

8. Storms, B. L. and Jang, C. S., "Lift Enhancement of an Airfoil Using a Gurney Flap and Vortex Generators," AIAA Paper 93-0647, Jan. 1993.

9. Rogers, S. E., "Efficient Simulation of Incompressible Viscous Flow over Single and Multi-Element Airfoils," AIAA Paper 92-0405, Jan. 1992.

10. Rogers, S. E., "Progress in High-Lift Aerodynamic Calculations," AIAA Paper 93-0194, Jan. 1993.

11. Rogers, S.E., and Kwak, D., "Upwind Differencing Scheme for the Time-Accurate Incompressible Navier-Stokes Equations," *AIAA Journal*, Vol. 28, No. 2, Feb. 1990.

12. Benek, J. A, Buning, P. G., and Steger, J. L., "A 3-D Chimera Grid Embedding Technique," AIAA Paper 85-1523, July 1985.

13. Jang, C. S., Ross, J. C., and Cummings, R. M., "Computational Evaluation of an Airfoil with a Gurney Flap," AIAA Paper 92-2708, June, 1992.

14. Baldwin, B. S., and Barth, T. J., "A One-Equation Turbulence Transport Model for High Reynolds Number Wall Bounded Flows," AIAA Paper 91-0160, Jan. 1991.

15. Chan, W. M., and Steger, J. L., "A Generalized Scheme for Three-Dimensional Hyperbolic Grid Generation," AIAA Paper 91-1586, June 1991.

16. Tramel, T. W. and Suhs, J. L., "PEGSUS 4.0 User's Manual," AEDC TR-91-8, June 1991.

17. Hicks, R. M. and Schairer, E. T., "Effects of Upper Surface Modification on the Aerodynamic Characteristics of the NACA 63_2-215 Airfoil Section," NASA TM 78503, 1979.

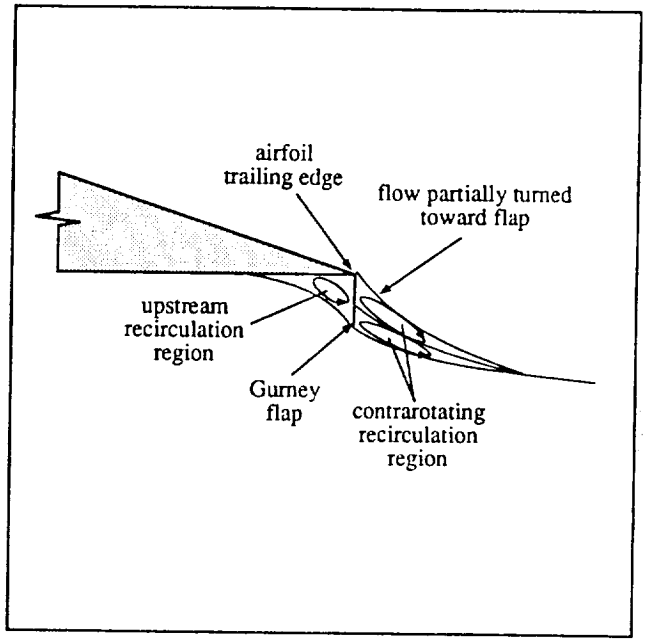

Fig. 1: Hypothesized trailing edge flow conditions for an airfoil with a Gurney flap (adapted from Ref. 4).

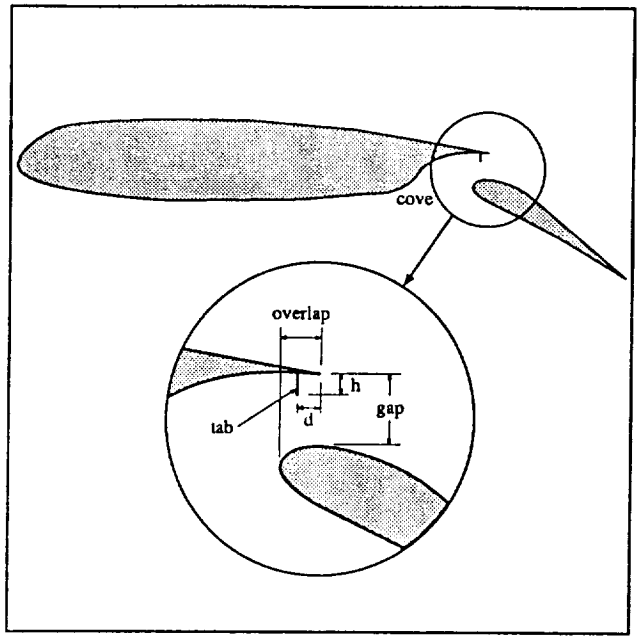

Fig. 2: Lift-enhancing tab geometry in main-element cove on two-element airfoil.

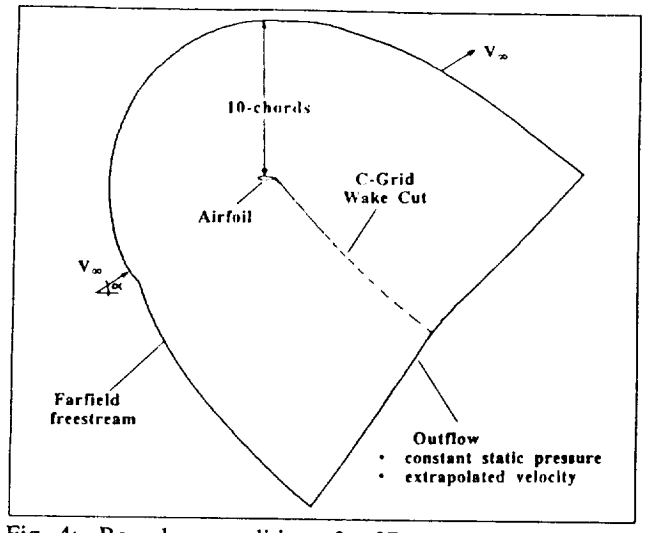

Fig. 4: Boundary conditions for 2D multi-element airfoil simulation in freestream flow.

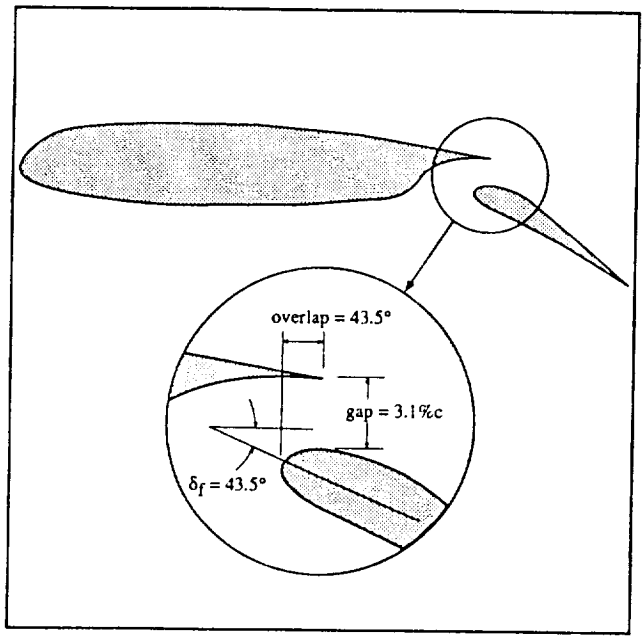

Fig. 3: Baseline two-element airfoil geometry (Ref. 5).

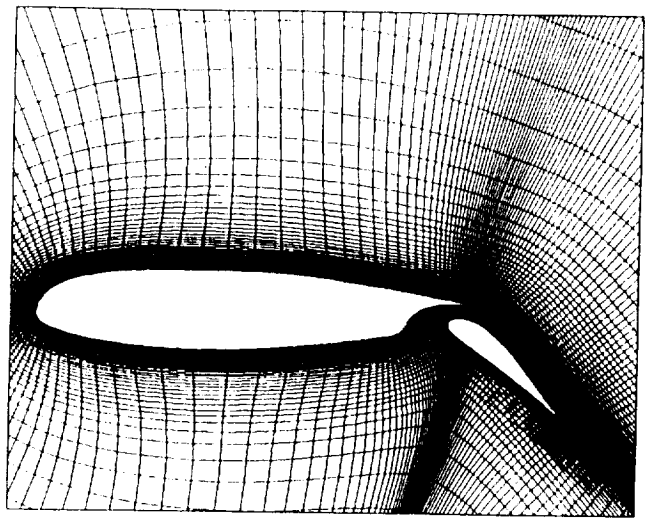

Fig. 5: Close-up of final two-element airfoil grid. Grid dimensions are 307 x 98 for the main-element and 155 x 42 for the flap.

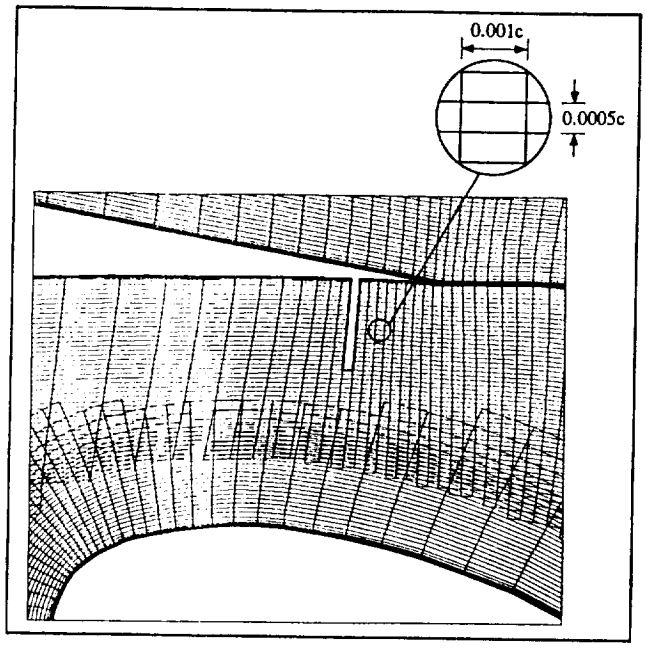

Fig. 6: Close-up of main-element cove showing grid resolution in the vicinity of a tab. Tabs of various size are created by "blanking-out" selected grid points.

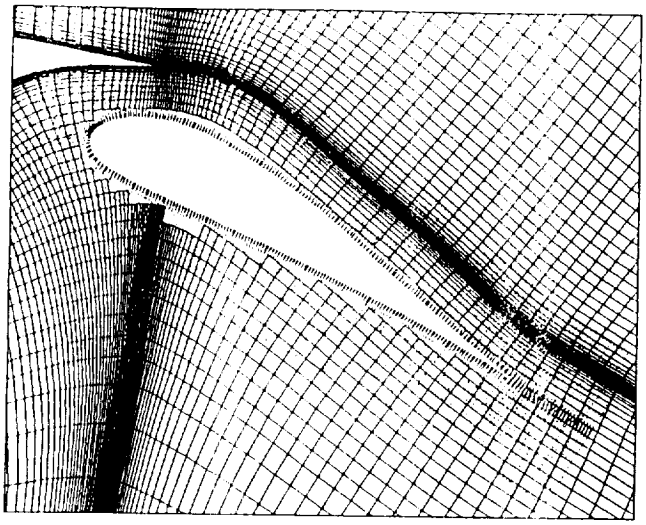

7a) Overlap region surrounding flap.

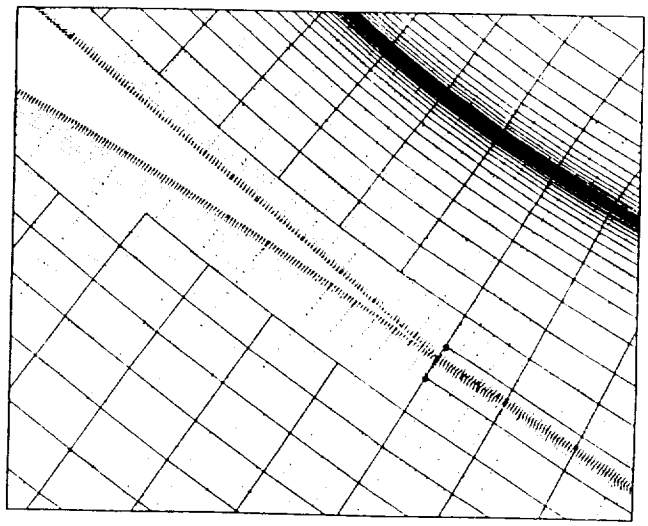

7b) Close-up of flap trailing edge; main-element fringe points are shown with larger dots.

Fig. 7: Initial two-element airfoil grid; main-element grid (solid lines), flap grid (dotted lines).

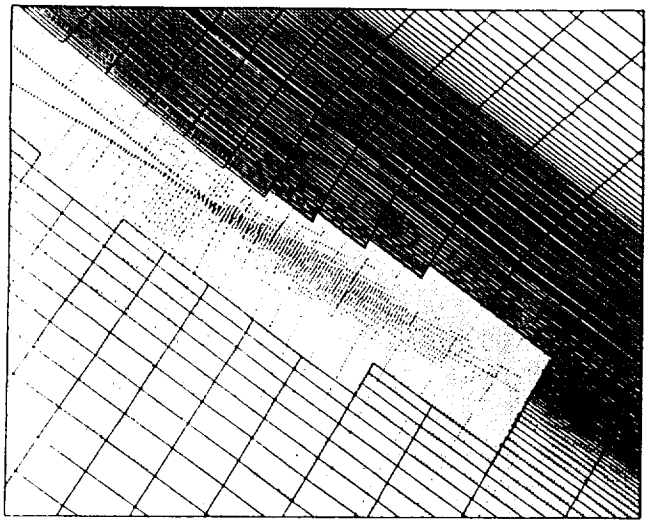

Fig. 8: Final two-element airfoil grid showing refinement near flap trailing edge.

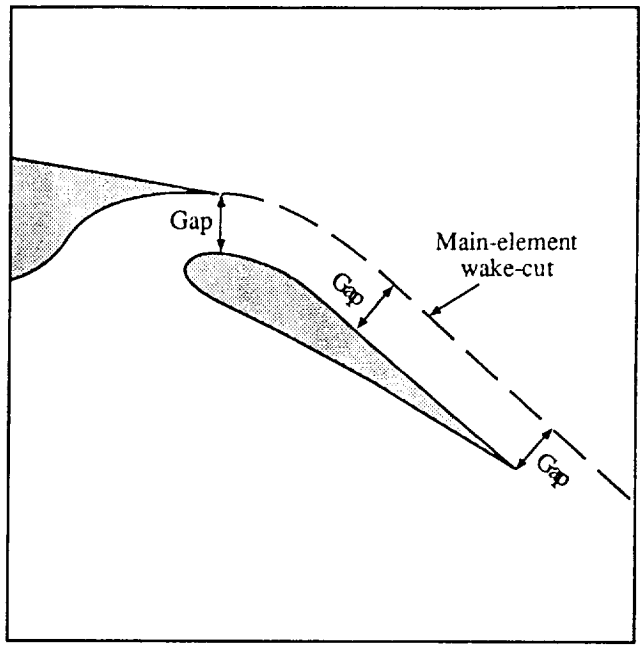

Fig. 9: Technique used to align main-element wake-cut with flap surface.

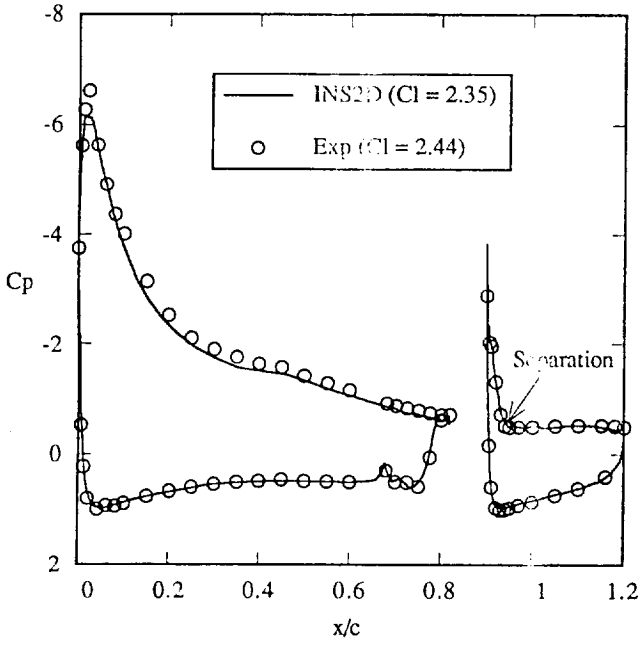

10a) Baseline airfoil with no tab, α=8.43°.

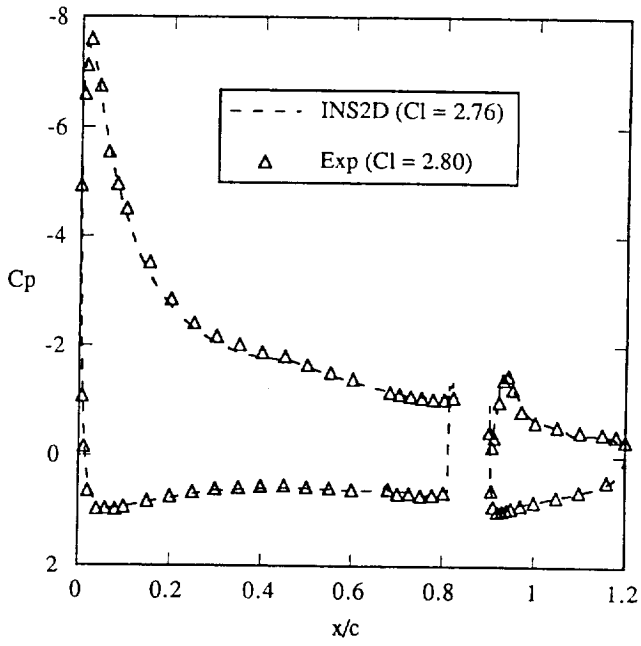

10b) Airfoil with 1%c tab at 1%c from trailing edge, α = 8.5°.

Fig. 10: Computed and measured pressure distributions for two-element airfoil; δf = 43.5°, gap = 3.1%c, overlap = 4.2%c, Re = 3.7 million.

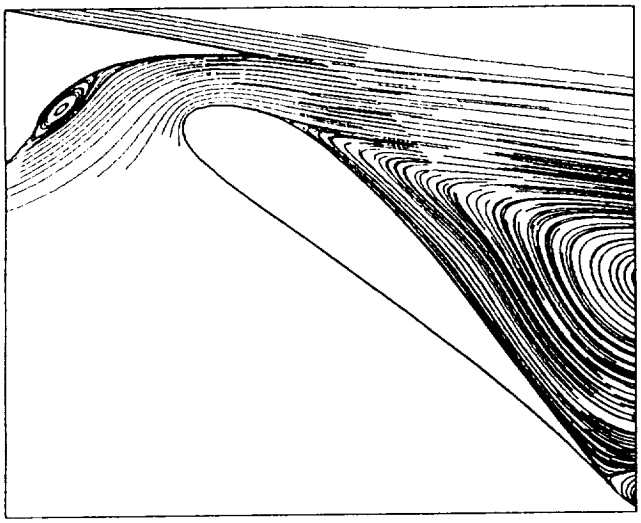

11a) Baseline airfoil with no tab, $\alpha = 8.43°$.

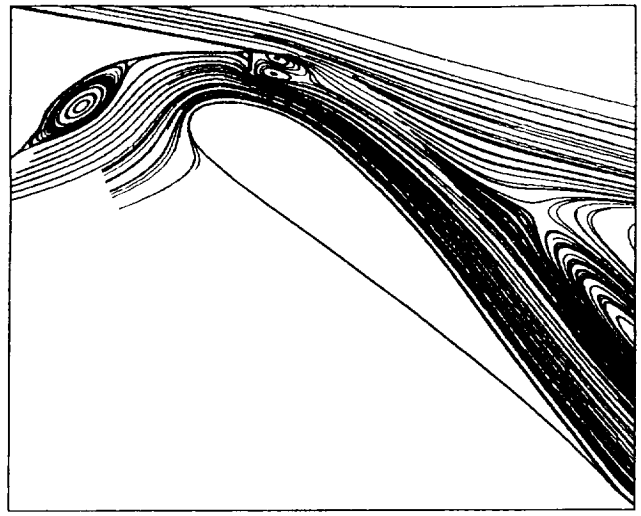

11b) Airfoil with 1%c tab at 1%c from trailing edge, $\alpha = 8.5°$.

Fig. 11: Computed streamlines near flap on two-element airfoil; $\delta f = 43.5°$, gap = 3.1%c, overlap = 4.2%c, Re = 3.7 million.

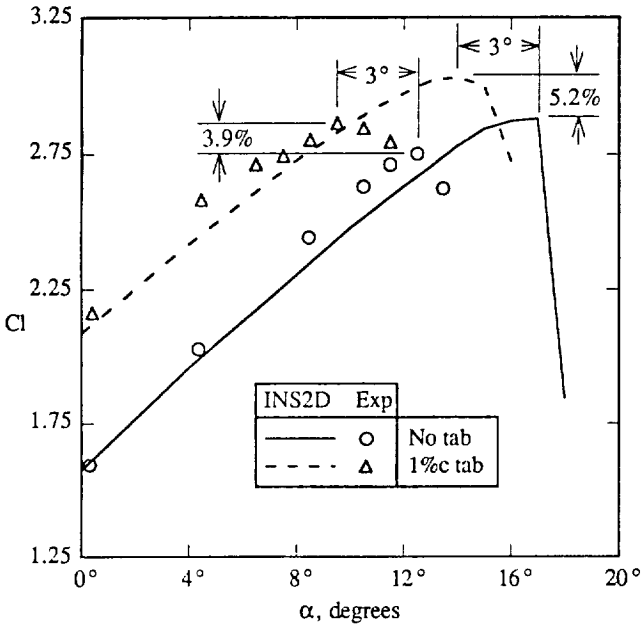

12a) Lift coefficient versus angle of attack.

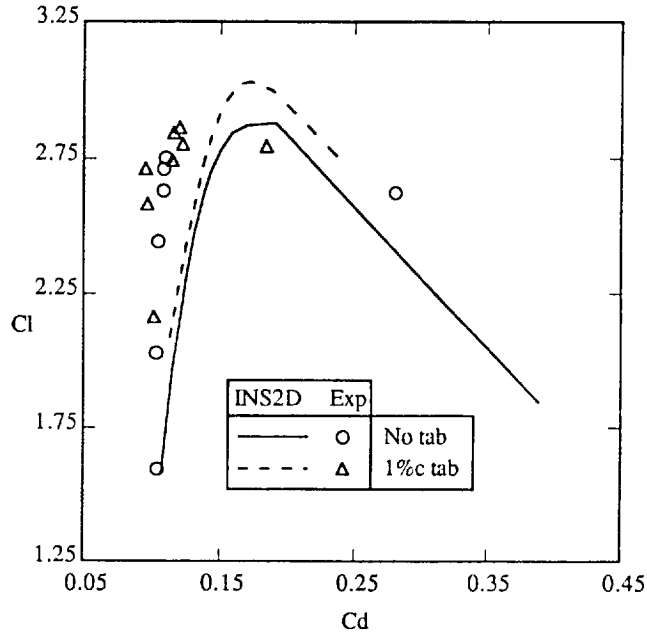

12b) Lift versus drag.

Fig. 12: Lift and drag of two-element airfoil with and without a 1%c tab; $\delta f = 43.5°$, gap = 3.1%c, overlap = 4.2%c, Re = 3.7 million.

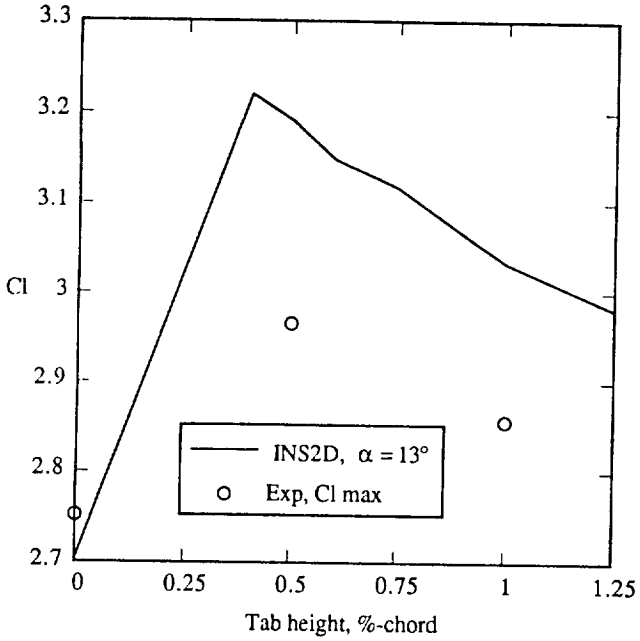

Fig. 13: Effect of tab height on lift; tab at main-element trailing edge on two-element airfoil, $\delta f = 43.5°$, gap = 3.1%c, overlap = 4.2%c, Re = 3.7 million.

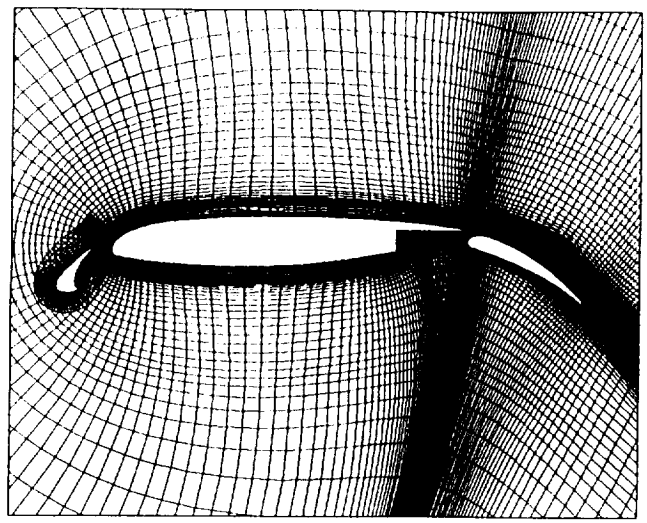

Fig. 15: Close-up of three-element airfoil grid. Grid dimensions are 121 x 31, 325 x 100, and 121 x 41, respectively, for the slat, main-element, and flap.

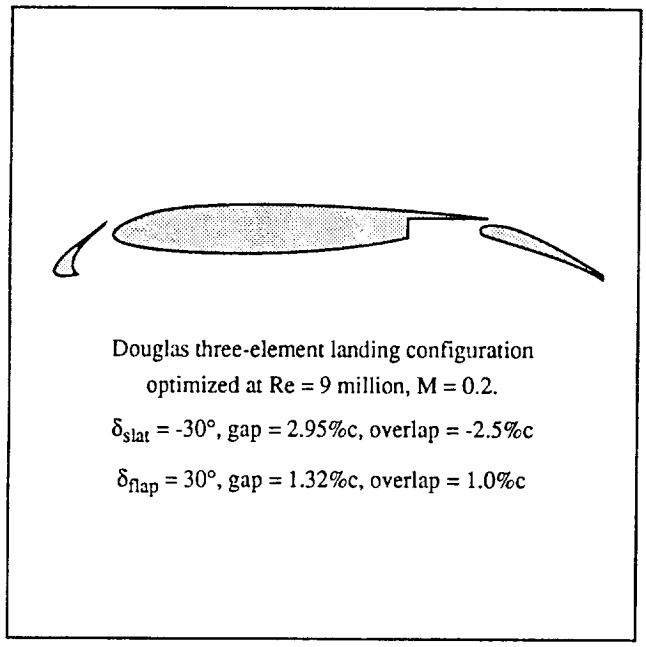

Fig. 14: Baseline three-element airfoil geometry (Ref. 1).

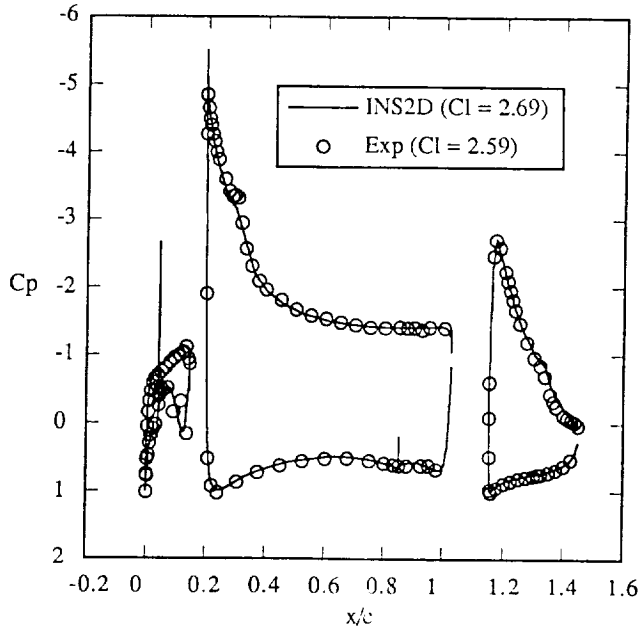

Fig. 16: Computed and measured pressure distributions for baseline three-element airfoil without a tab; optimized flap configuration, flap gap = 1.32%c, $\alpha = 4°$, Re = 9 million.

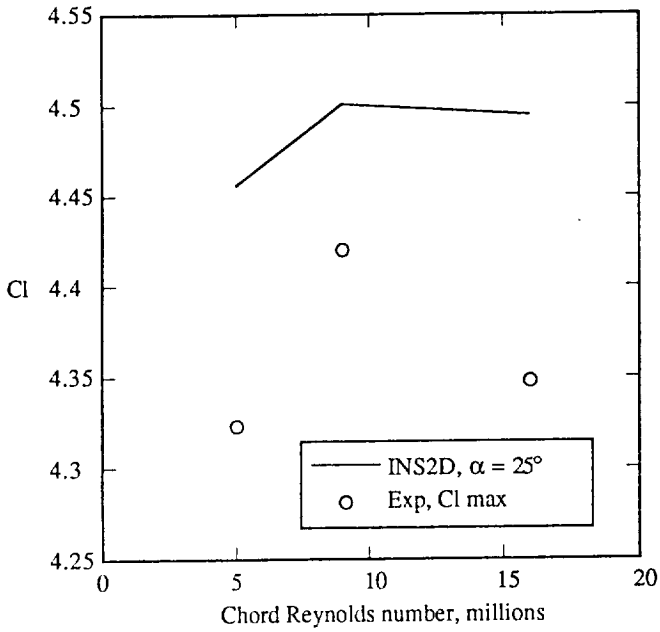

Fig. 17: Reynolds number effect on baseline three-element airfoil without a tab; optimized flap configuration, flap gap = 1.32%c.

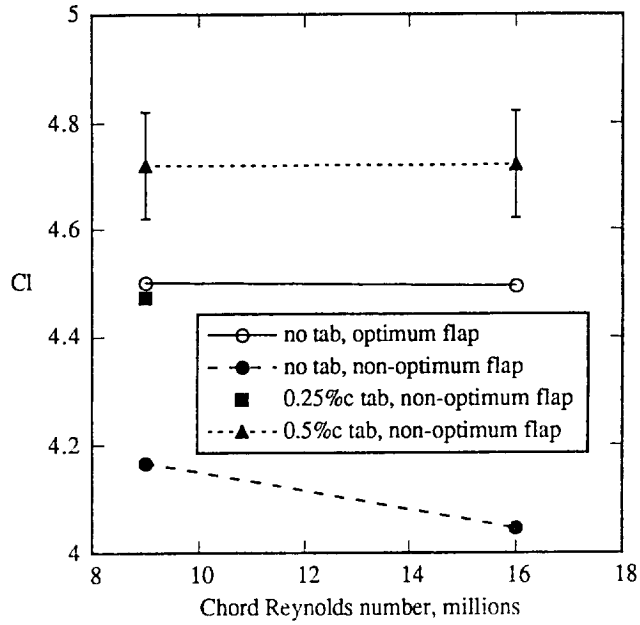

Fig. 18: Effect of tab height on lift; three-element airfoil, α = 25°.
Optimum flap configuration: δf = 30°, flap gap = 1.32%c.
Non-optimum flap configuration, δf = 45°, flap gap = 2.18%c.